Gaseous Plume Detection using Projective K-Means Method

Alex Cherekos

Chester F. Carlson Center for Imaging Science
Rochester Institute of Technology

ABSTRACT

This work is an extension of the invariant algorithm for detection and identification of gaseous plumes proposed by O'Donnell et al.[16,18] and explores the use of a subspace clustering technique to improve the detection of gaseous effluents. The hyperspectral pixels containing plume contributions should cluster near their representative background constituents due to the optically thin nature of gaseous plumes. Using this proposition we can improve the generation of the target basis vectors and automatically determine areas free of plume that can be used in the endmember characterization of the background.

1 INTRODUCTION

Detection and identification of gaseous effluent plumes and chemical agents are critical concerns in environmental monitoring and national security. The detection of fugitive gas and chemical agent spectra poses a challenge to the remote sensing community due to effects of the intervening atmosphere, the unknown spectral characteristics of the background, variations in gas plume temperatures and concentrations culminate into an unknown radiance contrast between the background and the plume. The gas spectral signature will manifest differently with variations in temperature, concentration, and backgrounds. The problem of detection and identification can be simplified somewhat by utilizing the long wave infrared portion (LWIR) of the electromagnetic spectrum where the target gases exhibit unique absorption features within this spectral range. In addition, the LWIR spectral region enables simplification of the governing equation by ignoring reflectance and scattering effects with the radiometric models.

Target detection in hyperspectral imagery typically utilizes a matched filter formulation where target spectral signatures are matched to an atmospheric corrected image yielding surface leaving spectral signatures. Alternate approaches use physics based modeling to propagate the target's ground leaving radiance through a similar atmosphere to the sensor. These algorithms forwardly predict the target spectral signatures to the sensor reaching radiance space by varying parameters in the physical model in order to model the expected target variability in the hyperspectral input. The spectral variability in the target and background spectra can be modeled using structured models where the data can be represented by linear combinations of endmembers or basis vectors.

In regards to gas effluent detection the target signature subspace is created using the absorption spectrum and by varying the gas concentration path length and the temperature contrast with the background surface material. The gas absorption spectrum is measured via laboratory means and through appropriate physical modeling the gas plumes at sensor radiance can be predicted using an atmospheric propagation model like MODTRAN.

GOVERNING EQUATION FOR THERMAL INFRARED

The radiometric model[15] for the effective thermal radiance reaching the sensor in the LWIR region can be expressed as:

$$L_\lambda = \left[\epsilon_{surface} B(\lambda, T_{surface}) + \left(F L_{d\varepsilon} + (1-F)\, L_{b\varepsilon}\right) r_{surface}\right] \tau_a + L_{u\varepsilon} = L_{surface}\tau_a + L_{u\varepsilon}$$

where $L_{surface}$ is the radiance headed towards the sensor attenuated by the atmospheric transmission (τ_a) along the target-sensor path and $L_{u\varepsilon}$ is the upwelling thermal emission from the sky. The thermal self-emission from the target is given by Planck's blackbody radiance equation:

$$B(\lambda,T) = \frac{2\alpha hc^2}{\lambda^5}\left(e^{\frac{hc}{\lambda kT}}-1\right)^{-1} \quad [W/(m^2 sr\mu m)]$$

$\alpha \equiv radiance\ units\ scalar = 1.0\cdot 10^{12}\ [\mu m^2/m^2]$ $h \equiv Planck's\ constant = 6.6256\cdot 10^{-34}\ [J\cdot s]$

$c \equiv speed\ of\ light = 2.9979\cdot 10^{14}\ [\mu m/s]$ $\lambda \equiv wavelength\ [\mu m]$

$k \equiv Boltzmann\ gas\ constant = 1.38\cdot 10^{23}\ [J/s]$ $T \equiv temperature\ [K]$

where the surface target thermal emission is given by:

$$L_T = \epsilon_{surface} B(\lambda, T_{surface}) .$$

The surface leaving radiance is the aggregation of the surface target thermal emission (L_T) and the reflected downwelling thermal emission from the sky ($L_{d\varepsilon}$) and background ($L_{b\varepsilon}$). For approximately horizontal surfaces the shape factor (*F)* is 1 and the background emission term can be eliminated yielding the following equation:

$$L_\lambda = [L_T + L_{d\varepsilon} r_{surface}]\tau_a + L_{u\varepsilon} = L_{surface}\tau_a + L_{u\varepsilon}$$

and for opaque target surfaces the diffuse reflectivity is given by:

$$r_{surface} = 1 - \epsilon_{surface}.$$

For a surface target with high emissivity approaching 0.99 the reflected downwelling radiance can be ignored, therefore the surface leaving radiance can be approximated solely by the surface target thermal emission (L_T) given above.

GOVERNING EQUATION FOR GASEOUS PLUMES

The radiometric model[9,17,18] for the effective thermal radiance reaching the sensor in the LWIR region containing a single intervening plume layer close to the surface of the Earth that can be modeled as:

$$L_\lambda = [L_T\tau_{plume} + L_{plume}]\tau_a + L_{u\varepsilon}$$

where the surface target thermal emission has been attenuated by the plume's transmission (τ_{plume}) and augmented by the thermal emission of the plume. The thermal emission of the plume can be approximated as:

$$L_{plume} = \epsilon_{plume} B(\lambda, T_{plume})$$

where $B(\lambda,T_{plume})$ is the blackbody radiance of the plume at temperature T_{plume}. The transmission of the plume is given by Beer's law:

$$\tau_{plume} = e^{-ck(\lambda,T_{plume})}$$

where c is the gas concentration path length [in ppm-m] and $k(\lambda,T_{plume})$ is the laboratory measured absorption spectrum [in 1/(ppm-m)] at temperature T_{plume}. If the plume is optically thin, the transmission can be approximated by:

$$\tau_{plume} = 1 - ck(\lambda, T_{plume})$$

Using Kirchoff's law and the law of conservation of energy the transmission and emissivity are related for a plume in thermodynamic equilibrium according to:

$$\tau_{plume} + \epsilon_{plume} + r_{plume} = 1$$

where r_{plume} is the reflectance of the plume. Since the gas particles are small compared to the wavelengths of interest (LWIR) the scattering caused by the plume can be ignored ($r_{plume} = 0$). Therefore the emissivity of the plume can be determined from the transmission by:

$$\tau_{plume} + \epsilon_{plume} = 1$$

where substituting for the transmission yields the emissivity of an optically thin plume containing a single gas constituent:

$$\epsilon_{plume} = ck(\lambda, T_{plume})$$

Combining the results yields the governing equation for the at-sensor radiance containing a single layer of gas:

$$L_\lambda = [L_T \tau_{plume} + \epsilon_{plume} B(\lambda, T_{plume})]\tau_a + L_{u\varepsilon}$$

$$L_\lambda = [L_T(1 - \epsilon_{plume}) + \epsilon_{plume} B(\lambda, T_{plume})]\tau_a + L_{u\varepsilon}$$

$$L_\lambda = [L_T - \epsilon_{plume} L_T + \epsilon_{plume} B(\lambda, T_{plume})]\tau_a + L_{u\varepsilon}$$

The gas will absorb a portion of the surface target thermal emission as governed by its absorption spectrum and concentration path length and also contribute a self-emission term to the radiance as seen by the sensor. The gas spectral signature required for detection is a function of these two terms and the temperature contrast with the surface. If the temperature of the gas is higher than the surface temperature the gas will be seen in emission; if the temperature of the gas is lower than the surface temperature the gas will be seen in absorption.

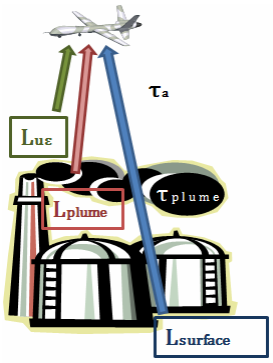

Figure 1. A depiction of the self-emission photon paths for the governing equation of gaseous plumes: $L_{surface}$ is the surface self-emission due to surface temperature attenuated by the transmission of the plume and atmosphere. Also included in the sensor reaching radiance is the self-emission of the gas plume (L_{plume}) and atmosphere ($L_{u\varepsilon}$).

2 BACKGROUND

The spectrum of an individual pixel tends to be a mixture of materials due to the projected size of the pixel onto the ground and the spatial variability of the scene content. The sensor integrates the radiance which is the superposition of a number of background materials and the atmosphere that separates the target from the sensor. Variations in the material surface, atmospheric conditions, sensor noise, and background interference cause an inherent spectral variability – the variability in the data can be model mathematically using linear mixing models[12-14]. In linear mixture models the spectral variability is confined to a convex hull where the observed spectrum can be represented by a linear combination of pure spectral endmembers:

$$x = \sum_{k=1}^{m} a_k s_k + w \equiv Sa + w$$

where the vectors s_k are assumed to be linearly independent and form the basis vectors that span the spectral variability of the hyperspectral dataset. The linear mixture model can be derived by placing constraints on a_k - these constraints restrict the observed spectral signatures to reside within a convex hull of unique deterministic spectral endmembers. The linear mixing model is given by:

$$x = \sum_{k=1}^{m} a_k s_k + w \equiv Sa + w$$
$$\sum_{k=1}^{m} a_k = 1 \quad (additive\ constraint) \qquad a_k \geq 0 \quad (positive\ constraint)$$

where a_k can now be interpreted as abundances of the k[th] endmember. The observed spectrum (x) that consists of a linear mixture of background and target endmembers is given by[12,13]:

$$x = \sum_{k=1}^{m} a_k s_k + w = \sum_{k=1}^{p} \tau_k t_k + \sum_{k=1}^{n} \beta_k b_k + w = T\tau + B\beta + w$$

where the p target endmembers (t_k) are stored in the columns of matrix T, the n background endmembers (b_k) are stored in the columns of matrix B, the vectors τ and β are the target and background abundances, and w is the residual error vectors.

2.1 SUBPIXEL TARGET DETECTION FORMULATION

Target detection algorithms[12,13] are formulated in statistical binary hypothesis testing where the two competing hypotheses are target absent and target present. It is ultimately a classification problem for very low probability of occurrence signatures where the decision is made regarding the observed spectrum (x) – the two competing hypotheses are:

$$H_0 : target\ present \qquad H_1 : target\ absent$$

If the conditional probabilities of the spectrum under the two hypotheses are known, the detection can be made using the likelihood ratio test. Detectors formulated using the likelihood ratio offer several key advantages: the detectors tend to minimize the risk associated with incorrect decisions and lead to constant false alarm rate detectors. If $f(x \mid H_0)$ and $f(x \mid H_1)$ are the conditional probability distribution functions of the spectrum x under the two hypotheses, the likelihood ratio test is given by:

$$LR = \frac{f(x|H_1)}{f(x|H_0)} \underset{H_0}{\overset{H_1}{\gtrless}} \eta$$

where the declaration of target present (rejection of the null hypothesis) can be made when the likelihood ratio exceeds the threshold η. The threshold determines the performance of the detector where the errors (misses and false alarms) should remain low and the correct decisions (hits and rejections) high. It is the compromise between two competing criteria – a low threshold to keep the probability of detection high and a high threshold to keep the probability of false alarms low. Due to the low abundance of targets – the detectors are geared to maximize only the probability of detection while keeping the false alarm rate under a predefined system tolerance. Autonomous detectors must determine the threshold automatically under *noise* and *background variations* and keep the false alarm rate constant as the conditions change. These detectors have desirable properties and are deemed CFAR detectors – CFAR detectors require modeling the detection statistic in the absence of targets in order to maximum the probability of detection of the system to a given false alarm rate. The threshold η is determined from the conditional probability of the detection statistics given the null hypothesis - where the right-tailed conditional probability is at the desired false alarm rate. The threshold η is given by:

$$P_{fa} = \int_{\eta}^{\infty} f(x|H_0)dx \leq constant$$

Since the parameters of the conditional probabilities of the spectrum under the two hypotheses are not known and must be estimated from the data using their maximum likelihood estimates, the detection test is formulated using the generalized likelihood ratio.

2.2 CFAR ADAPTIVE DETECTORS IN STRUCTURED BACKGROUNDS

The competing hypotheses[12,13] for structured background adaptive subpixel detectors are:

$$H_0 : x = B\beta_0 + w \qquad H_1 : T\tau + B\beta_1 + w = TB\gamma + w$$

where the matrix *TB* is the concatenation of the target and background endmembers. The detection is equivalent to choosing between the fits of two models: the linear mixture model using background endmembers only or the linear mixture model using the target and background endmembers. The generalized likelihood ratio test (GLRT) of the observed spectrum x is the ratio of the goodness of fit between the reduced model and full model and is given by:

$$D_{GLRT}(x) = \frac{x^T P_B^{\perp} x}{x^T P_{TB}^{\perp} x} = \frac{\left|\left|P_B^{\perp} x\right|\right|^2}{\left|\left|P_{TB}^{\perp} x\right|\right|^2} \underset{H_0}{\overset{H_1}{\gtrless}} \eta$$

where $P_A^{\perp}$ is the orthogonal projection onto the column space of the matrix A given by:

$$P_A^{\perp} = I - P_A \qquad P_A = A(A^T A)^{-1} A^T.$$

The orthogonal projection operator returns the residual vector between the original and column space projected vector. The magnitude of the residual vector is the sum of the squared errors between the original and projected vector. The numerator of the GLRT detector nulls/suppresses the background in the observed spectrum by projecting onto a subspace orthogonal to the background hyperplane; where the resulting residual vector can be conceived as potential target-like contribution. The denominator of the GLRT detector nulls/suppresses the target and background in the observed spectrum; the residual vector is the error term (*w*). If the observed spectrum is background only the detector statistic will yield a value near 1.0, if the observed spectrum contains a mixture of target and background the detector statistic will yield a value greater than 1.0.

2.3 INVARIANT TARGET DETECTION

The Healey-Invariant algorithm[15] was originally developed for the detection of a target spectrum under any illumination or atmospheric conditions. After using a physics-based radiative propagation model to predict the sensor reaching radiance of the target under a variety of conditions one can create a target subspace that spans this variability. The detector employing the invariant target subspace becomes increasingly more robust during detection since it has accounted for the expected in-scene variability of the targets.

O'Donnell et al.[16,18] extend the invariant algorithm to the problem of gas detection since the spectral signatures of gases vary with concentration, temperature, mixture ratios, and backgrounds. They use the forward model to predict the sensor reaching radiance of gases in both absorption and emission over a specified set of gas concentrations and gas/surface temperature differences. The radiometry model of a gas and surface radiance mixture is inherently nonlinear but can be expressed in linear form using an estimate of the background. In their approach the physics model used to generate the gas target radiance manifestation as seen by the sensor is:

$$L_{\lambda} = [B_{surface}(\lambda, T_{surface})\tau_{plume} + \epsilon_{plume} B_{plume}(\lambda, T_{plume})]\tau_a + L_{u\varepsilon}$$

$$T_{plume} = T_{surface} + \Delta T$$

where the surface is modeled as a blackbody with the mean of the maximum spectral brightness temperature of a region of pixels assumed free of the target gas. They employ the GLRT for each candidate gas species by modeling and characterizing the background using basis vectors generated from a target-free region representative of the background constituents.

2.4 TARGET AND BACKGROUND CHARACTERIZATION

Adaptive subpixel detectors[5,15] utilized in this study employ subspaces to characterize the invariant target and background spaces. The goal is to calculate a small set of basis vectors that span the variability in the physical model of the target spectra and the set of background (target-free) spectra selected from the input hyperspectral scene. Singular value decomposition (SVD) provides a factorization of the hyperspectral data arranged as columns of the matrix *Y*:

$$Y = USV^T$$

$$eigen(YY^T) \Rightarrow U, \lambda_U \qquad eigen(Y^TY) \Rightarrow V, \lambda_V$$

$$S \Leftarrow diag(\sqrt{\lambda_U}) \; or \; diag(\sqrt{\lambda_V})$$

where the matrix *U* contains the left singular vectors that span the range [column space] of the hyperspectral data in *Y*. The column space of a matrix gives the set of all possible linear combinations of its column vectors; in terms of the hyperspectral data matrix the column space represents all possible mixtures of the spectra. SVD returns a set of orthonormal basis vectors that span the convex hull of background or target spectra; the left singular vectors in U for either the target or background space should be selected to explain a high percentage of the overall variability.

3 APPROACH

3.1 SUBSPACE CLUSTERING

The goal behind subspace clustering[21] is to find several lower dimensional subspaces where each subspace represents a subset of the points in the n-dimensional space. The points will tend to cluster along several lower dimensional subspaces where fewer basis vectors can be used to span the points; as opposed to using a single set of basis vectors that span all of the points in a subspace of higher dimensionality. Subspace clustering should offer several advantages in hyperspectral target detection. It provides access to discovering the endmembers of the *real-world/in-scene* linear spectral mixtures within the hyperspectral dataset rather than permitting all possible combinations of a single set of endmembers that may or may not be applicable across the entire hyperspectral scene. Also, lower dimensional subspaces tend to limit the risk of target leakage into the background subspace – employing higher dimensional subspaces [than necessary] tend to increase the risk of the background and target spaces overlapping. In this research, subspace clustering is utilized to improve the generation of the target manifestations and background characterization. The hyperspectral pixels containing plume contributions should cluster near their representative background constituents due to the optically thin nature of gaseous plumes. The background subspace for each cluster partition is generated from an autonomously selected set of target-free spectra; in addition the mean value of the target-free spectra set is used as the surface self-emission in the gas target manifestation. It is believed that the customized target and background subspaces generated for each cluster partition should provide a more sensitive detection.

3.2 K-MEANS PROJECTIVE CLUSTERING

Points are assigned to the subspace S_i where the distance between the observation x and its closest point $\hat{x}$ in the available set of subspaces $S = \{S_1, \ldots, S_k\}$. The distance between the observation x and the subspace S_i is given by:

$$D(x, S_i) = ||x - P_{S_i} x||$$

where P_{S_i} is the projection onto the subspace given by:

$$P_{S_i} = S_i (S_i^T S_i)^{-1} S_i^T.$$

The observation x is assigned to the subspace yielding the minimal distance; note the distance can also be determined from the orthogonal projection operator given by:

$$D(x, S_i) = \sqrt{x^T P_{S_i}^{\perp} x} = \sqrt{x^T (I - P_{S_i}) x}.$$

Following the assignment of the points to their closest subspaces resulting in a partition of the data into clusters, the individual basis vectors that span the points in the cluster (P_i) is given by the singular value decomposition of the points in the cluster:

$$P_i = U_i S_i V_i^T$$

where the first q_i left singular vectors of U are chosen as the basis vectors for the cluster.

Algorithm: K-Means Projective Clustering (fixed dimensional subspaces)

Input: $X = \{x_1, \ldots, x_n\} \subseteq R^D$: set of n points in d-space.
$Q = \{q_1, \ldots, q_k\}$: set of dimensions for each of the k cluster partitions

Output: $P = \{P_1, \ldots, P_k\}$ *where* $X = \{P_1 \cup P_2 \cup \ldots \cup P_k\}$: points are partitioned into k clusters

$X \Rightarrow \{P_1, P_2, \ldots, P_k\}$: randomly assign input points to one of the k cluster partitions

While (convergence condition not satisfied) *do*
    Compute the optimal subspace for each cluster partition
    For i = 1 *to k do*
        $P_i = U_i S_i V_i^T$: compute the SVD of the points in the cluster
        $S_i \Leftarrow u_{i1}, \ldots, u_{iq_i}$: select the first q_i singular vectors of U to span cluster
    End
    $S = \{S_1, \ldots, S_k\}$: form the set of subspaces that span the k clusters
    Assign the points to the nearest subspace
    For i = 1 to *n do*
        $j = \underset{S=\{S_i, \ldots, S_k\}}{argmin} (D(x_i, S_j))$
        $P_j \Leftarrow x_i$: assign point to the j^{th} cluster partition
    End
End
Return $P = \{P_1, \ldots, P_k\}$

3.3 AUTONOMOUS IDENTIFICATION OF BACKGROUND SPECTRA

In order to prevent target leakage into the background subspace, target pixels should be removed from the set of spectra used to characterize the variability of the background. Since the first step in target detection involves a step to suppress the background any inclusion of target spectra will inhibit the detection. Often an area containing a representative set of the material constituents presumed free of targets is selected to characterize the background. During this research an algorithm to autonomously

identify the likely background spectra in each cluster partition was developed and used. The intent of the algorithm is not to identify all target-free locations with the input scene but to identify the representative set of background constituents.

Algorithm: Background Likely Ratio Test (BLRT)

Input: $P = \{P_1, \ldots, P_k\}$ and target gas specimen
Output: $B = \{B_1, \ldots, B_k\}$: set of background likely locations

$\hat{\lambda}_{free} \Leftarrow \epsilon_{plume} \leq \psi$: threshold gas specimen emissivity to identify spectral location free from dominant gas absorption or emission effects.

For each $P_i \in P$ *do* *; loop over each partition*
For each $x_j \in P_i$ *do* *; for each spectra assigned to the partition*
$T_j \Leftarrow Planck^{-1}(\hat{\lambda}_{free}, x_j)$: Invert Planck's equation to calculate maximum spectral brightness temperature in $\hat{\lambda}_{free}$
End
$T = \{T_1, \ldots, T_n\}$
$H_{temperature} = histogram(T, \kappa)$: compute histogram of the temperatures of the pixels assigned to the current cluster
$idx \Leftarrow where(H_{temperature} > 0)$: get the bins that occupied in the histogram
Foreach j in (idx)) do

; Compute representative background spectra compute either blackbody
; using surface temperature estimate or mean spectra of the locations
; previously marked background

$loc \Leftarrow where(B_i \cup T_j)$: find the spectra assigned to this temperature bin that have been previous marked as background
If $loc = \emptyset$ then
$L_{surface} = B(\lambda, T_j)$: compute blackbody using temperature of histogram bin j
Else
$L_{surface} = E\{P_i[loc]\}$: compute mean spectra of the location in the current partition
End

$L_{plume} \Leftarrow manifest(L_{surface})$: create target gas radiance using surface estimate

$T \Leftarrow basis(L_{target})$: compute basis for target subspace
$S \Leftarrow [L_{surface}, T]$: merge surface vector and target subspace

; compute the background likelihood ratio test for each pixel assigned
; to the partition
For each $x_j \in P_i$ *do*

$$D_{BLRT}(x_j) = \frac{\left|\left|P^{\perp}_{L_{surface}} x_j\right|\right|^2}{\left|\left|P^{\perp}_{S} x_j\right|\right|^2}$$

End

$B_i = D_{BLRT} \leq \phi_{gas}$: identify locations as background likely if under threshold
End

Repeat/Refine with second pass and merge results

End

The output of the BLRT statistic for the DIRSIG model scene containing a strong release of Freon gas is shown in Figure 3.3.1.

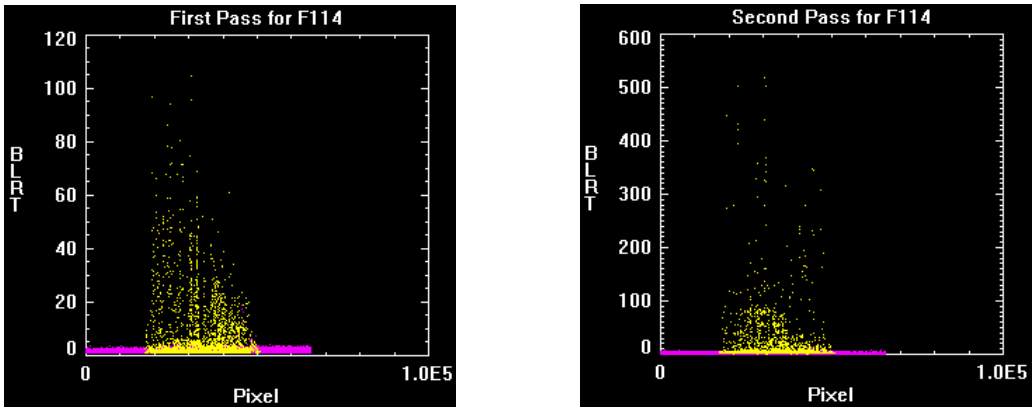

Figure 3.3.1. Plot of the BLRT statistics for DIRSIG modeled scene that includes a plume of Freon-114 gas released at 50 g/s. The BLRT statistics for plume locations are highlighted in yellow for the first and second pass of the background identification algorithm. The second pass of the algorithm boosts the background statistic and should increase the separability of strong target contributions and backgrounds.

4 RESULTS AND ANALYSIS

The performance of the algorithms employed in this project was tested against DIRSIG scenes having the same background scene elements but different gas target configurations. The input scenes were atmospherically corrected in a previous step; it should be noted that this can hinder the detection since the targets are optically thin – atmospheric correction could alter the target spectral signature and would diminish the likelihood of detecting atmospheric gases with the scene (e.g. ammonia).

Each DIRSIG scene was run through the subspace clustering step using a fixed dimensional subspace of three where the maximum number of partitions to return was set to twenty. The target detection utilized a reduced set of target (10) and background (minimum 10 and maximum 15) basis vectors. The target gas concentrations ranged from 0.1 [ppm m] to 3000 [ppm m] and temperature difference with the surface up to ± 30 [K]. The subspace partition's background likely locations were identified using the two pass BLRT algorithm with $\psi = 0.01$, $\kappa = 1.5$ [Kelvin] and $\varphi_{gas} = 1.7/1.9$. For each gas specimen in the candidate gas library, customized target and background subspaces were built for each partition in the input scene prior to the detection algorithm. The resulting GLRT detection cube was normalized using:

$$G = \{g_1, g_2, \ \cdots, g_n\}$$

$$\hat{G} = \frac{G}{\sqrt{\sum_{i=1}^{n} g_i^2}}$$

Table 4.1: DIRSIG scene gas configurations

Scene	Number of Plumes	Gas Species	Release Rate
Case 2	2	NH_3 – Ammonia, F114 – Freon 114	50 [g/s]
Case 3	1	F114 – Freon, TCE1122 - Tetrachloroethane	50 [g/s]
Case 4	2	NH_3 – Ammonia, F114 – Freon 114	0.25 [g/s]

Table 4.2: Enumeration of the gas species in GLRT detection cube

GLRT Index	Gas Name	GLRT Index	Gas Name
0	Fluorobenzene (C6H5F)	4	Ammonia (NH3)
1	1,2-Dichloropropane (DCLP12)	5	Phosgene (PHG)
2	Freon-114 (F114)	6	Sulfur hexafluoride (SF6)
3	Freon-125 (F114)	7	Tetrachloroethane (TCE1122)

4.1 CASE 2 ANALYSIS

Case 2 is a DIRSIG simulation of a SEBASS hyperspectral collection of a scene containing two separate plumes containing strong gas releases of Freon and ammonia – the input dataset contained 128 bands in the LWIR spectral range: 7.518 μm – 13.605 μm.

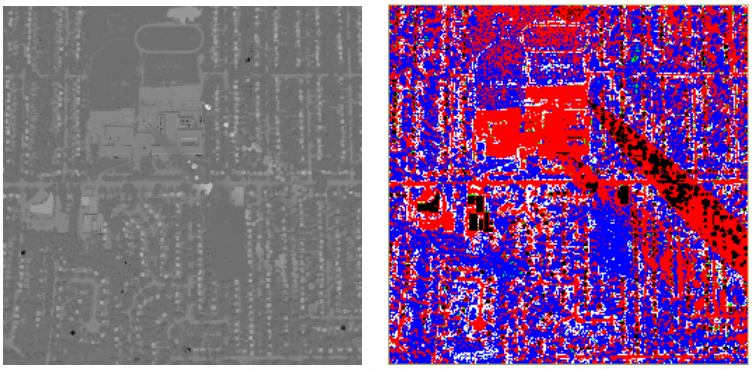

Figure 4.1.1. A band at 10.73 μm from the test scene that has been atmospherically corrected (left). The subspace cluster map depicts the partitions after 5 iterations [note the two plume structures]. The algorithm returned 5 partitions for the input hyperspectral scene (right).

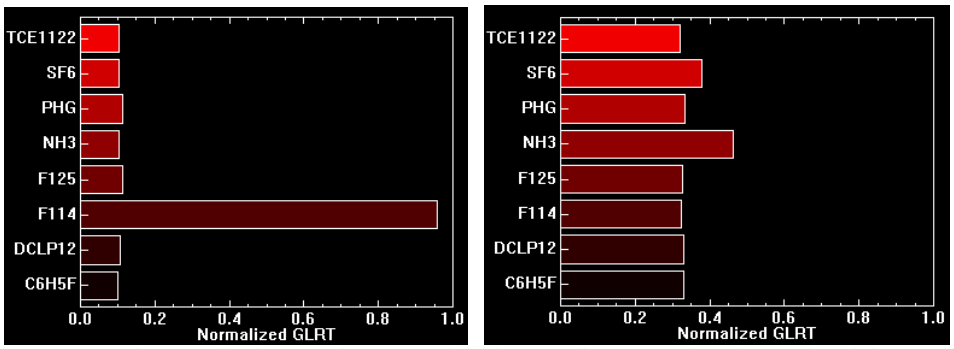

Figure 4.1.2. The normalized averaged GLRT statistic for a small area near the release point of the two plumes – the normalized GLRT statistic [plotted on the left] depicts Freon-114 as the most likely gas which corresponds to the truth data. The normalized GLRT statistic [plotted on the right] depicts Ammonia as the most likely gas which corresponds to the truth data.

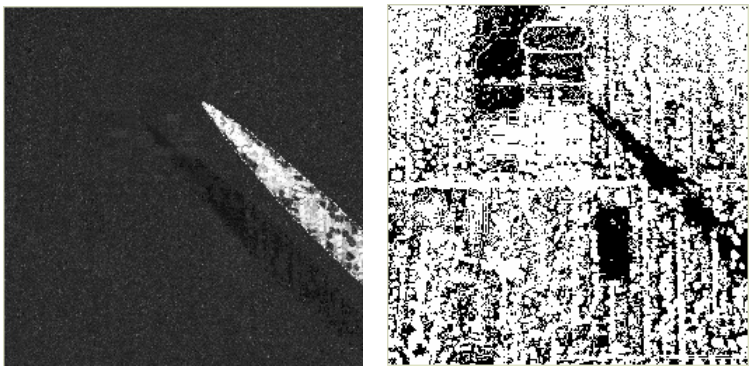

Figure 4.1.3. The normalized GLRT statistic for a successful Freon-114 detection is displayed on the left – the binary map used to identify spectra locations used in the characterization of the variability in the background is shown on the right.

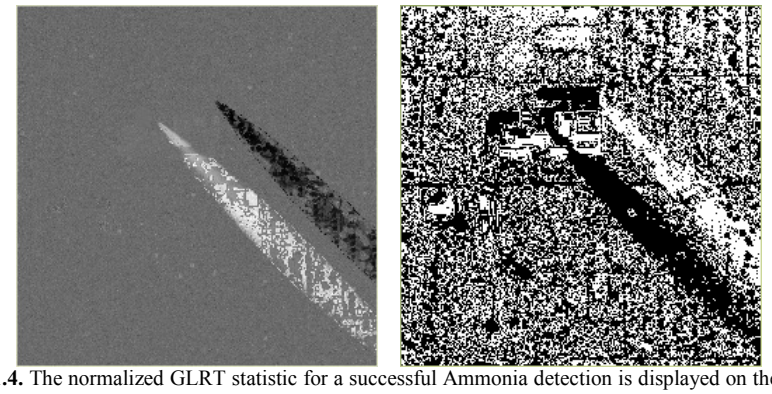

Figure 4.1.4. The normalized GLRT statistic for a successful Ammonia detection is displayed on the left – the binary map used to identify spectra locations used in the characterization of the variability in the background is shown on the right.

4.2 CASE 3 ANALYSIS

Case 3 is a DIRSIG simulation of a SEBASS hyperspectral collection of a scene containing a single plume containing a mixture of Freon and tetrachloroethane in a strong gas release configuration – the input dataset contained 80 bands in the LWIR spectral range: 7.98 μm – 12.004 μm. It is expected that the detection of tetrachloroethane should be impaired since several significant gas features outside the 12.004 μm spectral range have been excluded in the dataset.

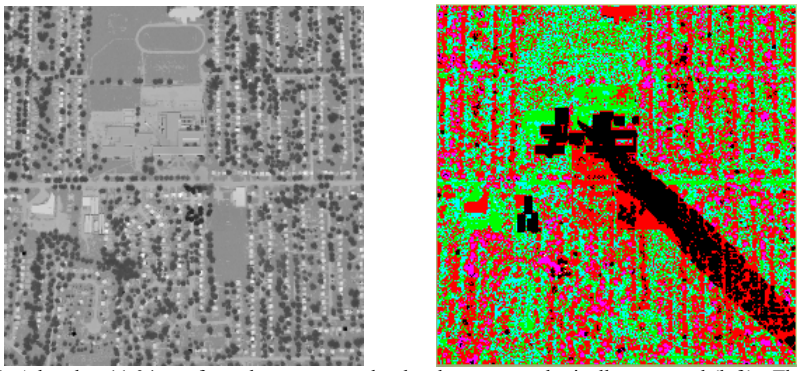

Figure 4.2.1. A band at 11.04 μm from the test scene that has been atmospherically corrected (left). The subspace cluster map depicts the partitions after 5 iterations [note the single plume structure]. The algorithm returned 6 partitions for the input hyperspectral scene (right).

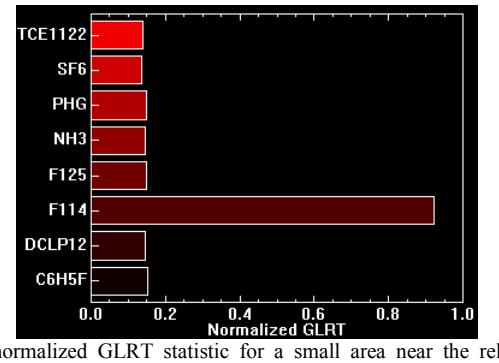

Figure 4.2.2. The average normalized GLRT statistic for a small area near the release point of the single two gas constituent plumes – the normalized GLRT statistic depicts Freon-114 as the most likely gas which corresponds to the truth data. However the second gas in the plume, tetrachloroethane was not sufficiently identified since the spectral bands excluded several significant gas features outside 12.004 μm.

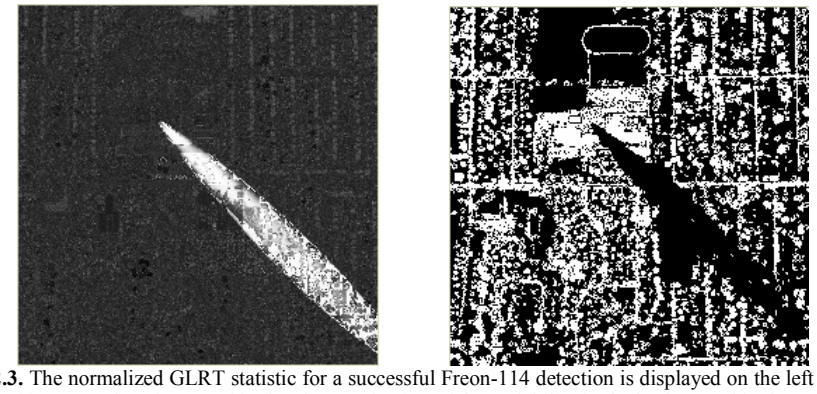

Figure 4.2.3. The normalized GLRT statistic for a successful Freon-114 detection is displayed on the left – the binary map used to identify spectra locations used in the characterization of the variability in the background is shown on the right.

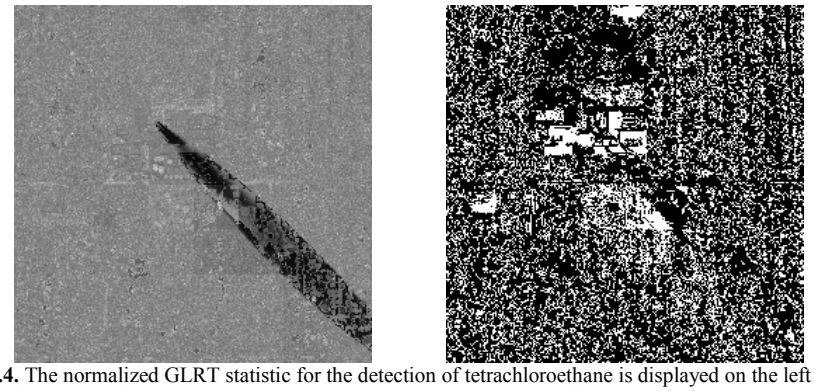

Figure 4.2.4. The normalized GLRT statistic for the detection of tetrachloroethane is displayed on the left – the binary map used to identify spectra locations used in the characterization of the variability in the background is shown on the right. The GLRT detection shows the expected minimal response in the locations of the plume.

4.3 CASE 4 ANALYSIS

Case 4 is a DIRSIG simulation of a SEBASS hyperspectral collection of a scene containing two separate plumes containing weak releases of Freon and ammonia – the input dataset contained 128 bands in the LWIR spectral range: 7.518 μm – 13.605 μm are included in the dataset. It is expected that the detection of ammonia should be impaired since the dataset has been atmospherically corrected prior to detection. Since ammonia is an atmospheric gas, atmospheric correction may alter the spectral signatures of the locations containing ammonia contributions.

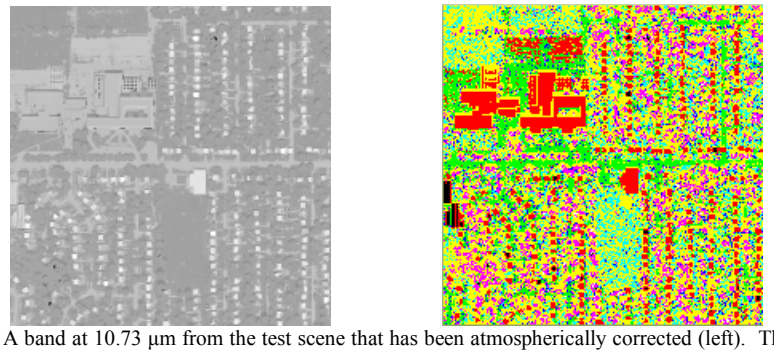

Figure 4.3.1. A band at 10.73 μm from the test scene that has been atmospherically corrected (left). The subspace cluster map depicts the partitions after 5 iterations [note no plume structures]. The algorithm returned 8 partitions for the input hyperspectral scene (right).

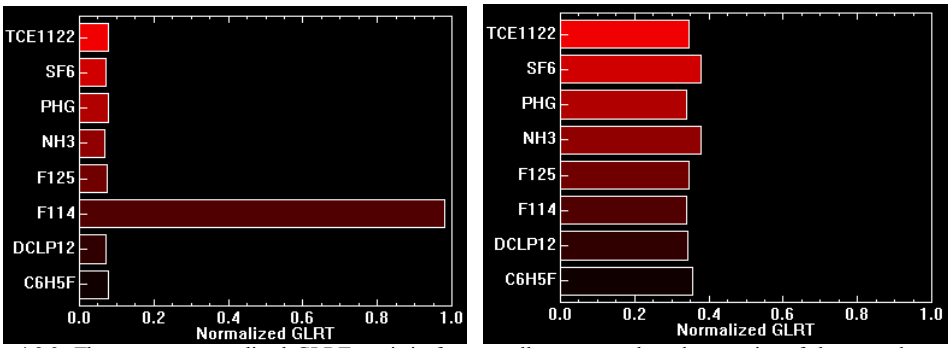

Figure 4.3.2. The average normalized GLRT statistic for a small area near the release point of the two plumes – the normalized GLRT statistic [plotted on the left] depicts Freon-114 as the most likely gas which corresponds to the truth data. The normalized GLRT statistic [plotted on the right] depicts Ammonia as the most likely gas which corresponds to the truth data.

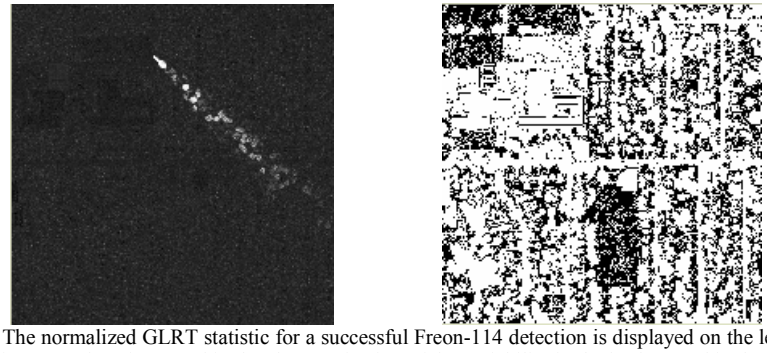

Figure 4.3.3. The normalized GLRT statistic for a successful Freon-114 detection is displayed on the left – the binary map used to identify spectra locations used in the characterization of the variability in the background is shown on the right.

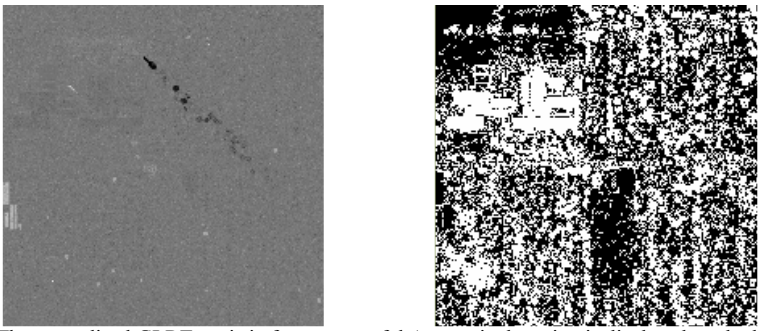

Figure 4.3.4. The normalized GLRT statistic for a successful Ammonia detection is displayed on the left – the binary map used to identify spectra locations used in the characterization of the variability in the background is shown on the right.

5 CONCLUSIONS

The detection and constituent analysis of gaseous plumes are important concerns in environmental monitoring and national security and poses a unique challenge to the airborne remote sensing community. This study investigated the use of subspace clustering and its application/extension to the gas detection algorithm proposed by O'Donnell. It has been demonstrated that subspace clustering can improve the detection of gas effluents since it provides a tool to solve two closely related problems inherent to the invariant method. Subspace clustering allowed the development of an algorithm to autonomously identify background pixels in each subspace partition – then use the subsequent set of locations to improve the estimate of the surface self-emission. It has been verified experimentally that using the mean value of the background likely spectra can improve the detection and has been demonstrated by the boost in the detection statistic in the second pass of the background identification algorithm. The algorithms developed in this study were shown to be effective in detecting the target gases in each DIRSIG scene.

APPENDIX A: GAS DETECTION RESULTS - UNNORMALIZED GLRT STATISTIC

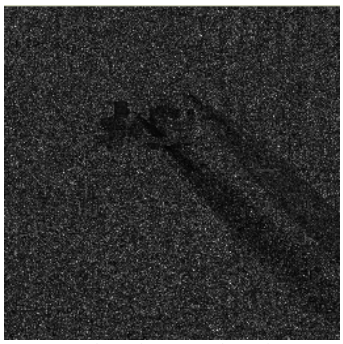

Figure A1. Fluorobenzene detection map for DIRSIG Case 2. Max value = 2.35

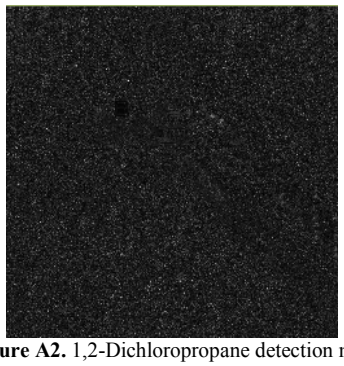

Figure A2. 1,2-Dichloropropane detection map for DIRSIG Case 2. Max value = 2.36

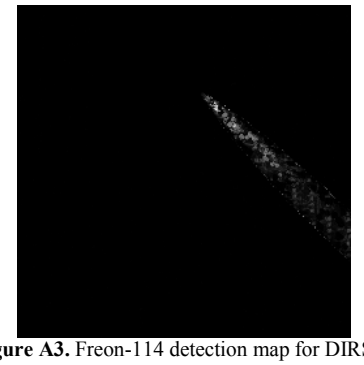

Figure A3. Freon-114 detection map for DIRSIG Case 2. Max value = 71.8

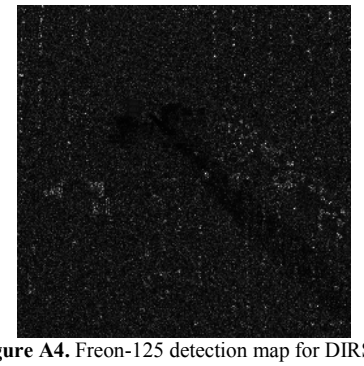

Figure A4. Freon-125 detection map for DIRSIG Case 2. Max value = 4.26

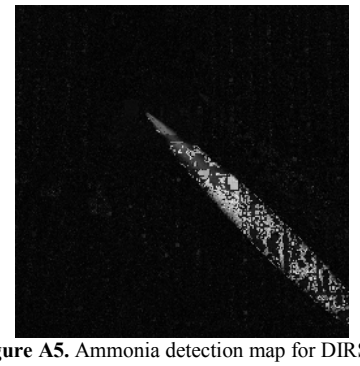

Figure A5. Ammonia detection map for DIRSIG Case 2. Max value = 3.52

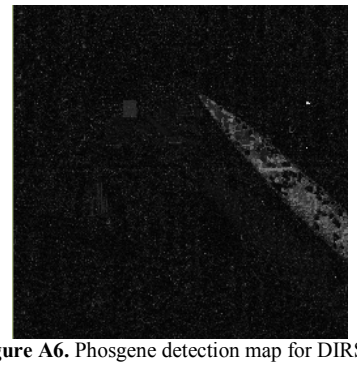

Figure A6. Phosgene detection map for DIRSIG Case 2. Max value = 3.01

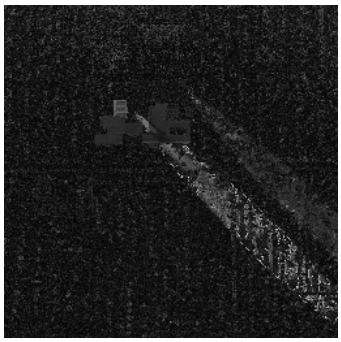

Figure A7. Sulfur hexafluoride detection map for DIRSIG Case 2. Max value = 2.09

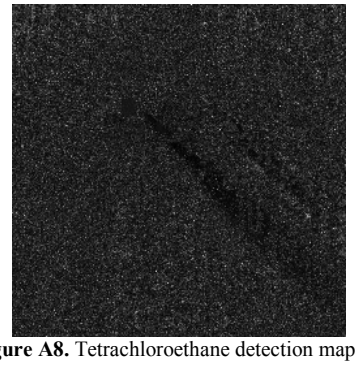

Figure A8. Tetrachloroethane detection map for DIRSIG Case 2. Max value = 2.14

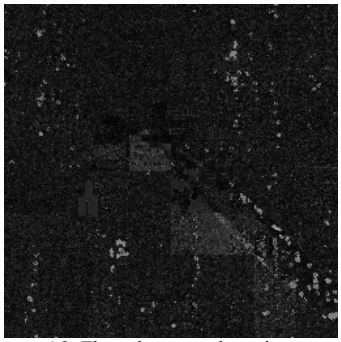

Figure A9. Fluorobenzene detection map for DIRSIG Case 3. Max value = 4.33

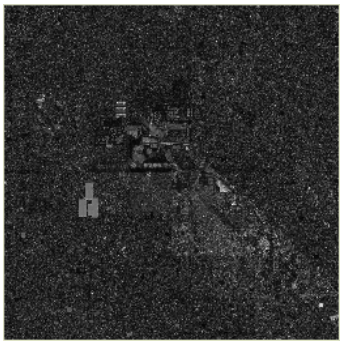

Figure A10. 1,2-Dichloropropane detection map for DIRSIG Case 3. Max value = 2.34

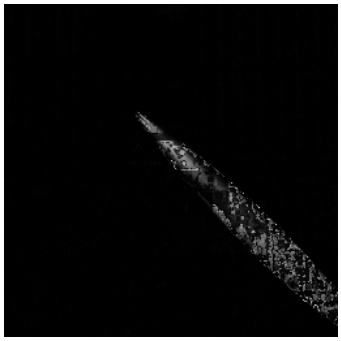

Figure A11. Freon-114 detection map for DIRSIG Case 3. Max value = 50.6

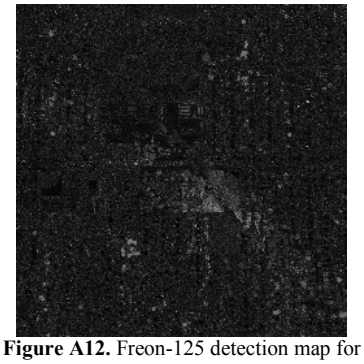

Figure A12. Freon-125 detection map for DIRSIG Case 3. Max value = 4.20

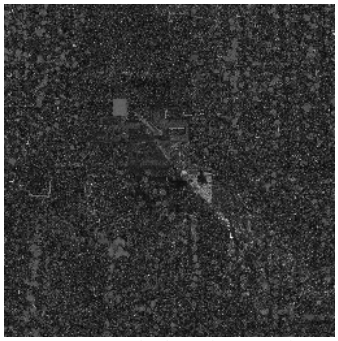

Figure A13. Ammonia detection map for DIRSIG Case 3. Max value = 1.98

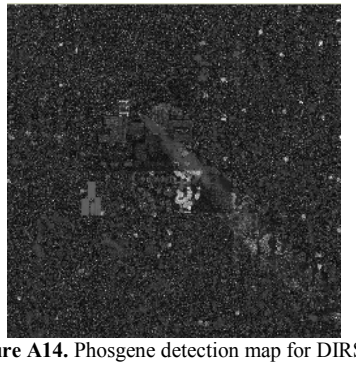

Figure A14. Phosgene detection map for DIRSIG Case 3. Max value = 2.19

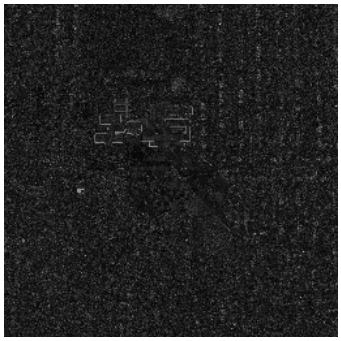

Figure A15. Sulfur hexafluoride detection map for DIRSIG Case 3. Max value = 2.43

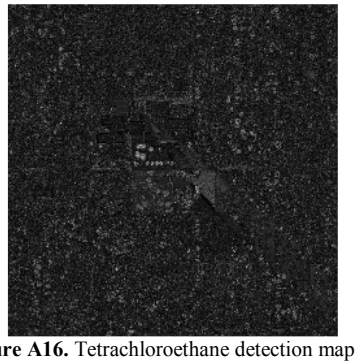

Figure A16. Tetrachloroethane detection map for DIRSIG Case 3. Max value = 2.78

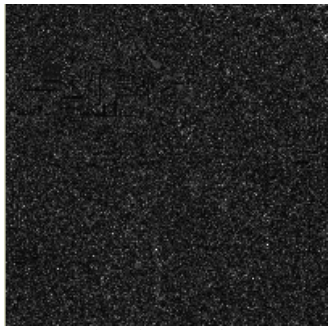

Figure A17. Fluorobenzene detection map for DIRSIG Case 4. Max value = 2.30

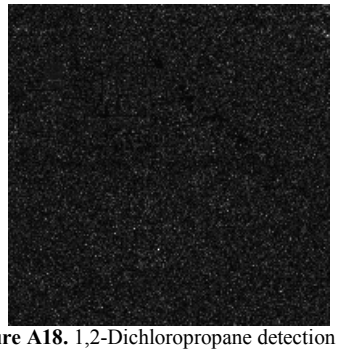

Figure A18. 1,2-Dichloropropane detection map for DIRSIG Case 4. Max value = 2.66

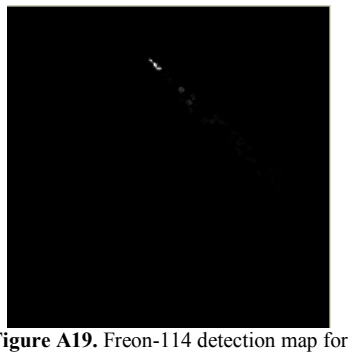

Figure A19. Freon-114 detection map for DIRSIG Case 4. Max value = 73.3

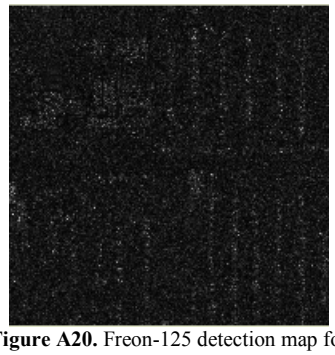

Figure A20. Freon-125 detection map for DIRSIG Case 4. Max value = 3.56

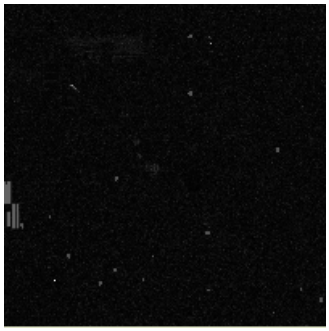

Figure A21. Ammonia detection map for DIRSIG Case 4. Max value = 3.40

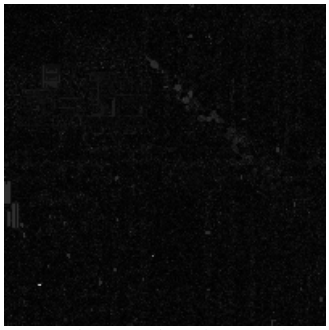

Figure A22. Phosgene detection map for DIRSIG Case 4. Max value = 3.67

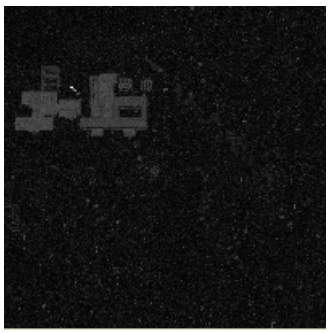

Figure A23. Sulfur hexafluoride detection map for DIRSIG Case 4. Max value = 2.19

Figure A24. Tetrachloroethane detection map for DIRSIG Case 4. Max value = 2.14

REFERENCES

1. Messinger D, "Gaseous plume detection in hyperspectral images: a comparison of methods," in *Algorithms and Technologies for Multispectral, Hyperspectral, and Ultraspectral Imagery X, Proceedings of SPIE, v. 5425*, pp. 592-603, 2004.

2. West J, Messinger D, Ientilucci E et al, "Matched filter stochastic background characterization for hyperspectral target detection," in *Algorithms and Technologies for Multispectral, Hyperspectral, and Ultraspectral Imagery XI, Proceedings of SPIE, v. 5806*, pp. 1 – 12, 2005.

3. Ientilucci E and Schott J, "Target Detection in a Structured Background Environment Using an Infeasibility Metric in an Invariant Space," in *Algorithms and Technologies for Multispectral, Hyperspectral, and Ultraspectral Imagery XI, Proceedings of SPIE, v. 5806*, pp. 491 – 502, 2005.

4. Hirsch E and Agassi E, "Detection of gaseous plumes in IR hyperspectral images using hierarchical clustering," in *Applied Optics, v. 46, no. 25*, pp. 6368-6374, 2007.

5. Bajorski P, Ientilucci E, and Schott J, "Comparison of Basis-Vector Selection Methods for Target and Background Subspaces as Applied to Subpixel Target Detection," in *Algorithms and Technologies for Multispectral, Hyperspectral, and Ultraspectral Imagery X, Proceedings of SPIE, v. 5425*, pp. 97 – 108, 2004.

6. Harsanyi J C, Chang C, "Hyperspectral Image Classification and Dimensionality Reduction: An Orthogonal Subspace Projection Approach," in *IEEE Transactions on Geoscience and Remote Sensing, v. 32, no. 4,* pp. 779-785, 1994.

7. Funk C C, Theiler J, Roberts D A et al, "Clustering to improve matched filter detection of weak gas plumes in hyperspectral thermal imagery," in *IEEE Transactions on Geoscience and Remote Sensing, v. 39, no. 7,* pp. 1410-1420, 2001.

8. Farley V, Chamberland M, Lagueux P, et al, "Chemical Agent Detection and Identification with a Hyperspectral Imaging Infrared Sensor," in *Imaging Spectrometry XII, Proceedings of SPIE, v. 6661,* pp. 1-9, 2007.

9. Theiler J, Foy B, and Fraser A, "Characterizing non-Gaussian clutter and detecting weak gaseous plumes in hyperspectral imagery," in *Algorithms and Technologies for Multispectral, Hyperspectral, and Ultraspectral Imagery XI, Proceedings of SPIE, v. 5806*, pp. 182 – 193, 2005.

10. Manolakis D, Model J, Rossacci M, et al, "Software Algorithms for False Alarm Reduction in LWIR Hyperspectral Chemical Agent Detection," in *Algorithms and Technologies for Multispectral, Hyperspectral, and Ultraspectral Imagery XIV, Proceedings of SPIE, v. 6966*, pp. 1-11, 2008.

11. Manolakis D, Jairam L G, Zhang D and Rossacci M, "Statistical Models for LWIR Hyperspectral Backgrounds and their Applications in Chemical Agent Detection," in *Algorithms and Technologies for Multispectral, Hyperspectral, and Ultraspectral Imagery XIII, Proceedings of SPIE, v. 6565*, pp. 1 – 12, 2007.

12. Manolakis D and Shaw G, "Detection algorithms for hyperspectral imaging applications" in *Signal Processing Magazine, IEEE, v. 19, no. 1,* pp. 29-43, 2002.

13. Manolakis D, Marden D and Shaw G, "Hyperspectral Image Processing for Automatic Target Detection Applications," in *Lincoln Laboratory Journal, v. 14, no. 1,* pp. 79-116, 2003.

14. Manolakis D, Shaw G and Keshava N, "Comparative Analysis of Hyperspectral Adaptive Matched Filter Detectors," in *Algorithms and Technologies for Multispectral, Hyperspectral, and Ultraspectral Imagery VI, Proceedings of SPIE, v. 4049*, pp. 2 – 17, 2000.

15. Schott John R. , Remote Sensing: The Image Chain Approach 2nd Edition, Oxford University Press, USA, 2007.

16. O'Donnell E, Messinger D, Salvaggio C and Schott J, "The invariant algorithm for identification and detection of multiple gas plumes and weak releases," in *Algorithms and Technologies for Multispectral, Hyperspectral, and Ultraspectral Imagery XI, Proceedings of SPIE, v. 5806*, pp. 206 – 217, 2005.

17. Messinger D, Salvaggio C and Sinisgalli N, "Detection of gaseous effluents from airborne LWIR hyperspectral imagery using physics-based signatures," in *International Journal of High Speed Electronics and Systems,* pp. 1-11, 2006.

18. O'Donnell E, Messinger D, Salvaggio J and Schott J, "Identification and detection of gaseous effluents from hyperspectral imagery using invariant algorithms," in *Algorithms and Technologies for Multispectral, Hyperspectral, and Ultraspectral Imagery X, Proceedings of SPIE, v. 5425*, pp. 573 – 582, 2004.

19. Pogorzala D, Messinger D, Salvaggio C and Schott J, "Gas plume species identification by regression analyses," in *Algorithms and Technologies for Multispectral, Hyperspectral, and Ultraspectral Imagery X, Proceedings of SPIE, v. 5425,* pp. 583 – 591, 2004.

20. Pogorzala D, Messinger D, Salvaggio C and Schott J, "Gas plume species identification in airborne LWIR imagery using constrained stepwise regression analyses," in *Algorithms and Technologies for Multispectral, Hyperspectral, and Ultraspectral Imagery XI, Proceedings of SPIE, v. 5806,* pp. 194 – 205, 2005.

21. Agarwal P and Mustafa N, "k-Means Projective Clustering," in *Principles of Database System, ACM SIGMOD,* pp. 155-165, 2004.